J. J. Wynne
J. A. Armstrong

Systematic Behavior in Alkaline Earth Spectra: A Multichannel Quantum Defect Analysis

"Two-electron" atoms are more complex than "one-electron" atoms because of electron-electron interactions. This leads to spectra that are not well understood. Using multiple photon excitation and ionization detection, we have extensively studied Rydberg series of states in Ca, Sr, and Ba. The spectroscopic data were interpreted by using multichannel quantum defect theory (MQDT). In this context, systematic trends in the atom series Ca, Sr, and Ba are discussed.

Introduction

The revolution in optical spectroscopy, driven by the tunable laser, has spawned a renaissance in atomic spectroscopy. This is a field with a long and continuing history of achievements. However, the unique capabilities provided by tunable lasers have allowed new and exciting studies of the electronic structure of atoms. We have been studying the high Rydberg states in the alkaline earth atoms Ca, Sr, and Ba. These atoms have two valence electrons outside a closed, rare-gas-like electronic shell and are therefore classified as two-electron atoms. As such, they provide a "laboratory" for the study of the effects of electron correlation on atomic spectra and atomic structure. This "laboratory" is well matched to the capabilities of tunable dye lasers because it is possible to use a small number of visible or near-visible photons to selectively excite and study well-defined Rydberg series of states converging on the first and several higher ionization limits of these atoms.

Many aspects of the electronic structure of many-electron atoms are still not well understood. The simplest picture of such atoms is that each electron moves in a well-defined orbit, independent of the other electrons. However, spin-orbit coupling effects and Coulomb repulsion between electrons modify this picture, and lead to admixtures of configurations and splitting of terms that depend on the relative orientations of total orbital angular momentum L and total spin S. These effects hamper our ability to identify the states of many-electron atoms and to classify them with one-electron labels. When one looks at tabulations of atomic energy levels [1], there are obvious large gaps in the list of known members of many Rydberg series. Laser spectroscopy offers the possibility of enormously extending our knowledge of these series.

In a series of papers [2–4] we have reported on laser spectroscopic investigations of extensive Rydberg series of different types in Ca, Sr, and Ba. Similar studies have been reported by several European groups [5–8]. Previous to the laser-assisted work, studies of these atoms by absorption spectroscopy [9–11] had yielded extensive information on the $^1P_1^o$ Rydberg series. Multichannel quantum defect theory (MQDT), a method developed by Seaton [12] and by Fano and coworkers [13–16], has proven to be very useful in analyzing these spectroscopic data [2–4, 6, 8, 17].

In this paper we briefly review our laser spectroscopic methods but *our main point is a discussion of the systematic trends in the alkaline earths that our MQDT analyses have uncovered.* In particular, MQDT extracts from complicated spectra a small set of parameters that describes, in a compact manner and with surprising accuracy, the details of these spectra. What we have found in each case analyzed is that for a spectrum of given J and parity, all but one of the set of parameters are nearly the same for Ca, Sr, and Ba. This similarity goes well beyond what has been previously recognized from comparisons of state-

Copyright 1979 by International Business Machines Corporation. Copying is permitted without payment of royalty provided that (1) each reproduction is done without alteration and (2) the *Journal* reference and IBM copyright notice are included on the first page. The title and abstract may be used without further permission in computer-based and other information-service systems. Permission to *republish* other excerpts should be obtained from the Editor.

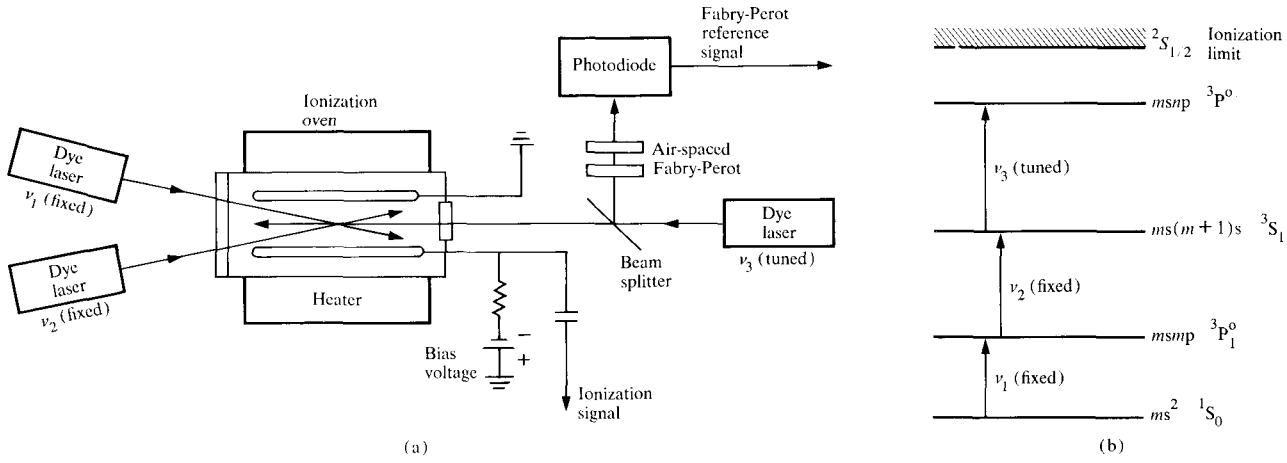

Figure 1 (a) Experimental setup for multiphoton ionization spectroscopy (MIS). (b) Energy level diagram of typical alkaline earth atom showing three-photon sequence that excites $^3P^o$ states.

by-state analyses of the spectra. An earlier analysis by Lu [18] briefly considered systematic trends in the alkaline earths.

Multiphoton ionization spectroscopy (MIS)

The tunable dye laser as a spectroscopic tool gives the experimenter the ability to start with atoms in a known state, *e.g.*, the ground state, and excite them along a carefully chosen excitation pathway. The pathway is determined by both the photon energies and the laser polarization. Of course, such selective excitation is possible with nonlaser light sources, but the vastly superior spectral brightness of laser light allows a large fraction of the excited atoms to end up in a single final state. This is true even when the excitation involves more than one photon. Such selective multiphoton excitations were, in effect, not observable before the advent of lasers. By using combinations of tunable lasers, Rydberg series that are not connected to the ground state by one-photon transitions may be observed and identified. For example, the use of an even number of photons leads to final states of the same parity as the ground state. Such states cannot be observed in absorption from the ground state by electric dipole transitions. In general, with tunable lasers we can excite and observe final states of a particular pre-selected symmetry.

In our work on the alkaline earths, we have used a simple experimental setup to detect excitation to high Rydberg states. Our technique is based on detection of ionization that follows population of a high Rydberg state by multiphoton excitation, hence the name multiphoton ionization spectroscopy (MIS). The essence of MIS is illustrated in Fig. 1. A pipe containing the atomic species of interest is heated to provide adequate vapor pressure ($\approx$10–100 Pa). For the alkaline earths Ca, Sr, and Ba, a typical operating temperature is 800°C, at which temperature the pipe is red-hot. One or more laser beams [three are shown in Fig. 1(a)] are aimed into the pipe to spatially overlap between a pair of parallel-plate ionization-detecting electrodes. The detection mechanism, which has been known for over 50 years [19], is based on neutralization of the space charge that is produced by thermionic emission of the heated electrodes. With a negative dc bias voltage applied to one of the electrodes, a dc current flow of thermionically emitted electrons occurs. If the bias voltage is small enough, a significant space charge is established, with its maximum density near the negative electrode. If positive ions are introduced into the gas, they partially neutralize the space charge, allowing more electrons to flow between the electrodes. Due to the much greater drift velocity of the electrons than the ions (approximately inversely proportional to their respective masses), many extra electrons flow from the negative to the positive electrode while each positive ion is traveling from the positive to the negative electrode. In addition, the positive ions may become trapped near the maximum of the space charge density, prolonging their lifetime and allowing proportionally more electron current. The net result is a gain of $\approx 10^5$ in the extra charge flowing in the external circuit due to the introduction of positively charged ions into the vapor between the electrodes. Such a detector, called a space-charge-limited thermionic diode, provides us with a simple and convenient method for detecting

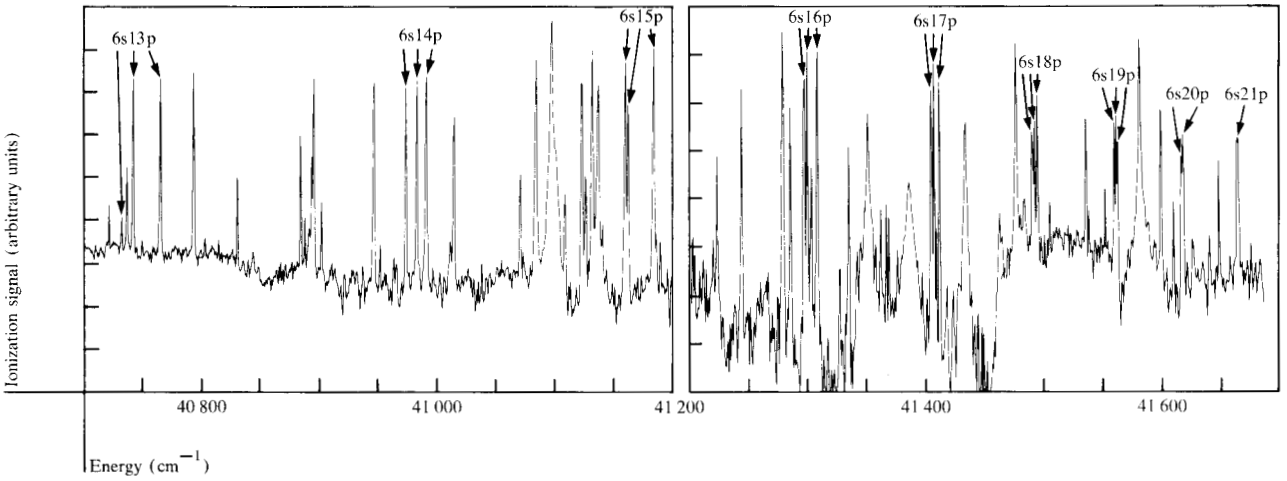

Figure 2 Multiphoton ionization spectrum of Ba. The labels correspond to the members of the 6snp series, with the arrows designating various terms (*e.g.*, $^3P_1^o$, $^3P_2^o$, $^1P_1^o$). The ionization limit is 42034.9 cm^{-1}.

ionization in the hot atomic vapor. The resulting signal is linear in the number of ions over a dynamic range of several orders of magnitude.

The mechanism by which the ions are produced requires some explanation. In our studies of bound Rydberg states, the laser photons excite the atoms to a final bound state. Once this final state is populated it must still be ionized to give a signal. Of the possible photo- or collisional ionization mechanisms, we believe that the predominant one is chemi-ionization, *i.e.*, the production of stable molecular ions upon collision of an excited atom with a ground state atom. This conclusion is based on optical spectroscopic observations of atomic ions showing that these ions last only $\approx$100 μs, whereas the conductive species responsible for the ionization signal lasts for $\approx$1 ms [20]. Furthermore, recent multiphoton ionization studies carried out in an atomic beam of Sr have detected the production of Sr_2^+, in support of the chemi-ionization mechanism [21].

To record a spectrum, one of the lasers is scanned and the ionization signal recorded. In the setup shown in Fig. 1(a), ν_1 and ν_2 are held fixed while ν_3 is scanned. Part of the beam at ν_3 is split off and passed through a Fabry-Perot interferometer, providing a reference signal. The transmission through the Fabry-Perot is periodic in ν_3, showing peaks at fixed frequency spacing of $c/2\ell$, where c is the speed of light and ℓ is the air-space thickness between the two plates of the interferometer. Once this spacing is calibrated against known peaks in the ionization signal, it provides a frequency marker against which the frequencies of unknown peaks in the ionization spectrum can be calibrated. The signals may be recorded on chart paper or stored digitally in a computer.

Figure 2 shows a spectrum of Ba that was recorded by using three lasers (as in Fig. 1). This spectrum is representative of many such spectra that we have recorded for Ca, Sr, and Ba. For the purposes of this article, the most important things to point out about Fig. 2 are that there is an excellent signal-to-noise ratio and that most of the peaks represent states of Ba that have not been previously identified or classified. The reader is referred to Refs. [2–4] for more details about the experimental methods and for presentations of the extensive new data.

Multichannel quantum defect theory (MQDT)

Traditional analyses of atomic spectra have been aimed at the determination of the energies of the initial and final states of one-photon transitions, the strengths of such transitions, and the classification of the states. When Rydberg series are noninteracting, as in alkali metal ("one-electron") atoms, this classification is relatively straightforward. However, when the series are strongly interacting, as in "many-electron" atoms, such classification becomes difficult. In many cases classifications of states by a pure configuration are wrong. Each state may be instead a mixture of several configurations. However, the mixture describing one state is *not* unrelated to the mixtures describing the other states of the same series. This important fact is recognized by MQDT, which analyzes the spectra in terms of interactions between entire series instead of between individual configurations.

A full exposition here of what MQDT is and why it works would take us too far afield. The important point for the reader of this article to appreciate and keep in mind is that there is a new way of analyzing complex spectra and that the result of this analysis is a small set of parameters that gives a highly accurate and compact de-

scription of the spectra. As noted earlier, all but one of the parameters describing a given spectral type are nearly invariant along the atom series Ca, Sr, and Ba. We believe that this near-invariance reflects dynamical symmetries in the electron-electron interaction of the two outermost electrons.

Because we wish to present results based on our MQDT analyses, we must define certain terms, especially the parameters of MQDT. However, on the basis of the following short definitions the reader is not expected to understand the details of MQDT; those wishing to pursue a deeper understanding are referred to Refs. [2, 13–16].

The first term we need to define is *channel*. A channel is a group of states that encompasses both a region of discrete energies and a continuum. One type of channel, known as a collision- or i-channel, describes a set of states with an outer electron of various energies, an electronic core in a definite energy level, specific angular momenta of the outer electron and the core, and their coupling. This type of channel is an appropriate description of the atom when the Rydberg electron is far from the core. As an example, in Ba the $6sn\mathrm{p}\ {}^1\mathrm{P}_1^o$ discrete states and the $6s\epsilon\mathrm{p}\ {}^1\mathrm{P}_1^o$ continuum together constitute an L, S-coupled collision channel. Another type of channel, known as an eigen- or α-channel, diagonalizes the noncentral part of the electron-electron interaction. This type of channel is an appropriate description of the atom when the Rydberg electron is close to or penetrating the core.

Interactions among channels are described by MQDT in terms of a small number of physically meaningful parameters whose values may be derived from experimental measurements. These parameters represent the effects of the electronic core on the wave function of the excited electron. They are: 1) the elements of a unitary matrix $U_{i\alpha}$ that specifies the transformation diagonalizing the matrix for noncentral scattering of the excited electron by the core; 2) the eigendefects μ_α that specify the eigenvalues of the scattering matrix, $\exp(i2\pi\mu_\alpha)$; and 3) the electric dipole matrix elements D_α that describe transitions from a given discrete state, such as the ground state, to each eigenchannel. The U-matrix transforms a basis set of α-channels to a basis set of i-channels.

An important role is played in MQDT by effective quantum numbers ν_i, defined in terms of equations of the type

$$E = I_i - R/(\nu_i)^2, \tag{1}$$

where E is the measured energy of a state, I_i is the ith ionization threshold (or series limit) of the atom, and R is the Rydberg constant appropriate for the atom in question. The essence of MQDT is an analytical relationship, parametrized in terms of $U_{i\alpha}$ and μ_α, between the ν_i:

$$\det |U_{i\alpha} \sin \pi(\nu_i + \mu_\alpha)| = 0. \tag{2}$$

For an N-limit, M-channel problem, there are N equations of the type given by Eq. (1); $U_{i\alpha}$ is an $M \times M$ matrix and there are M eigendefects μ_α. The solution to Eq. (2) is an $(N-1)$-dimensional surface Σ in the N-dimensional ν_i-space. This surface is parametrized in terms of $U_{i\alpha}$ and μ_α.

Our work has dealt primarily with finding values for $U_{i\alpha}$ and μ_α such that Eqs. (1) and (2) fit our experimental data when expressed in terms of ν_i. We have carried out this fitting with the graphical aid of Lu-Fano plots [22]. These plots present a graph of ν_i *versus* ν_j for various pairs of effective quantum numbers. One finds as many values of ν_i as there are relevant series limits in the spectra of interest. This number is the same as the number of distinct core states in the configurations that are admixed in the spectrum.

Systematic behavior in the series Ca, Sr, and Ba

Up to this point we have been reviewing and summarizing our earlier work as an introduction to what we now present. We have found that the values of $U_{i\alpha}$ and μ_α that give good MQDT parametrizations of the experimental data on Rydberg series are intimately related to one another along the atom series Ca, Sr, and Ba. Thus, for example, if we consider the ${}^1\mathrm{P}_1^o$ series of these three atoms, we find a common subset of these parameters that describes the channel interactions *in all three atoms* between the $ms n\mathrm{p}$ and $(m-1)\mathrm{d}n'\mathrm{p}$ channels.

We note that Be and Mg are not included in this set of alkaline earth atoms. The difference between Be and Mg and the heavier alkaline earths is that the latter have low-lying empty d shells in the electronic core, allowing for the possibility of low-lying core-electron excitations to d states. This common feature seems to lie at the root of the systematic behavior we will be discussing. We believe that this observed systematic behavior also extends to the heaviest alkaline earth Ra; however, there are not yet sufficient data to be certain. (See the discussion in the next section.)

The common subset of parameters gives the *shape* of the surface Σ as distinct from its *position*. This subset consists of the U-matrix and a set of new combinations of eigendefects numbering one less than the original set. The "omitted" parameter is the average eigendefect

$$\bar{\mu} = \left(\sum_{\alpha=1}^{M} \mu_\alpha\right)/M, \tag{3}$$

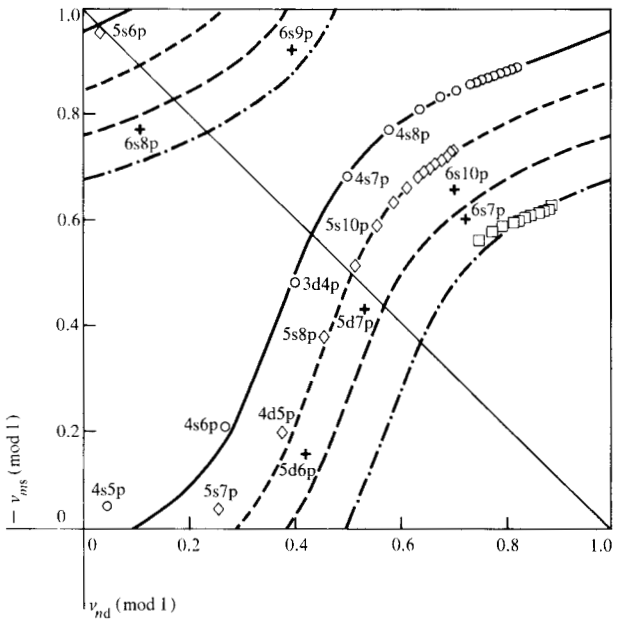

Figure 3 Lu-Fano plots for the bound $^1P_1^o$ spectra of Ca (——, ○) Sr (- - -, ◇), Ba (— —, +), and Ra (— •—, □). The curves are MQDT fits using the parameters given in Table 1. Intersections of the curves with the diagonal line give the μ_1 (upper left-hand curves) and μ_2 (lower curves) values. The integers m (see ordinate) are 4(Ca), 5(Sr), 6(Ba), and 7(Ra). The integers n (see abscissa) are 3(Ca), 4(Sr), 5(Ba), and 6(Ra).

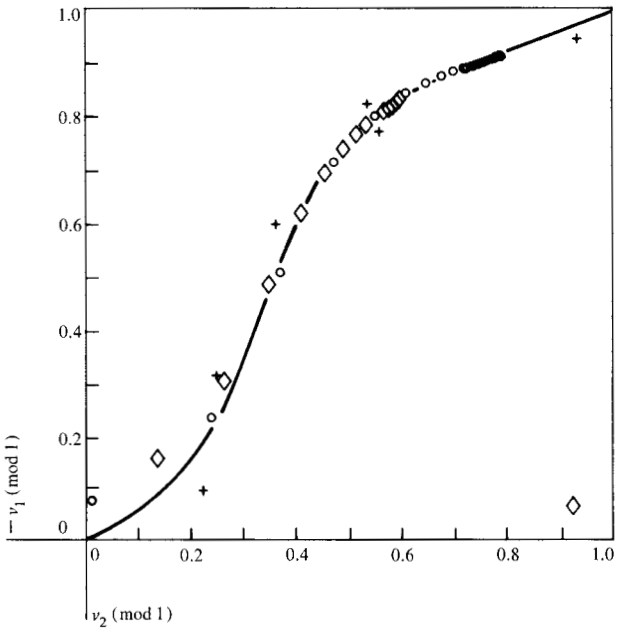

Figure 4 Composite Lu-Fano plot produced by displacing the curves and data of Fig. 3 along the diagonal so as to superimpose the curves. Data points are shown for Ca (○), Sr (◇), and Ba (+).

and it alone changes substantially from atom to atom. A representation of the new eigendefect parameters is found by taking $\mu_\alpha' = \mu_\alpha - \bar{\mu}$ and substituting this into Eq. (2), which now reads

$$\det |U_{i\alpha} \sin \pi(\nu_i + \mu_\alpha' + \bar{\mu})| = 0. \tag{4}$$

If we also take $\nu_i' = \nu_i + \bar{\mu}$ and substitute this into Eq. (4), we have

$$\det |U_{i\alpha} \sin \pi(\nu_i' + \mu_\alpha')| = 0. \tag{5}$$

What we have done in the transformation is displace Σ *along the N-space body diagonal* ($\nu_1 = \nu_2 = \cdots = \nu_N$) *a distance* $\bar{\mu}$. *This displacement does not change the shape of the surface* Σ.

We now assert that the shape of Σ corresponds to the interaction among channels and that this shape is nearly constant within a given spectrum along the series Ca, Sr, and Ba. Thus we will allow the surfaces fitting the data to be displaced along the body diagonal to see how well they may be superimposed for these three atoms. We believe that the constancy of the shape of Σ mirrors invariances in the dynamics of the correlated "two-electron" system along the series Ca, Sr, and Ba. We shall now show by a series of examples how this procedure works.

• $^1P_1^o$ *spectra*

As a first example we consider the spectral series seen in absorption from the ground state. The main series correspond to the $ms^2\ ^1S_0$-$msnp\ ^1P_1^o$ transitions. The spectra are complicated by interactions between the $msnp$ and $(m-1)dn'p$ channels. Thus the real states of the $^1P_1^o$ series are mixtures of these two types of configurations. From the MQDT point of view, this is a two-limit, two-channel problem. In the i-channel representation, we have channel 1 consisting of the electronic core in the ms state and the Rydberg electron in a p state. Channel 2 consists of the core in the $(m-1)$d state and the Rydberg electron in a p state. In both channels the electron angular momenta are coupled to produce a $^1P_1^o$ state. To treat these spectra we need experimental values for the energies E of the real states and values for the ionization limits I_1 and I_2. These may be found in the literature [1, 4, 9–11]. For I_2 we take the average of the two limits $I_{2D_{3/2}}$ and $I_{2D_{5/2}}$, corresponding to the lowest excited d states of the alkaline-earth ions. Thus we ignore spin-orbit effects. This is an approximation which depends on the fact that the spin-orbit splitting of the D core is small compared to the energy required to excite the core from an S to a D state, and our result is here applied only to the bound spectra below the I_S limit. Next we calculate values for ν_1 and ν_2 by using Eq. (1). For these simple two-channel cases, it is appropriate to present Lu-Fano plots in the form $-\nu_1$(mod 1) *versus* ν_2(mod 1), *i.e.*, to plot the

Table 1 Two-channel MQDT parameters for various states using I_S and I_D.

Parameter	$^1P_1^o$				$^3P_1^o$			$^3D_2$		
	Ca	*Sr*	*Ba*	*Ra*	*Ca*	*Sr*	*Ba*	*Ca*	*Sr*	*Ba*
Θ	0.60	0.60	0.60	0.60	0.30	0.30	0.30	0.25	0.25	0.25
μ_1	0.97	0.89	0.83	0.76	0.97	0.90	0.85	0.86	0.80	0.78
μ_2	0.57	0.49	0.43	0.36	0.87	0.80	0.75	0.35	0.29	0.27
$\Delta = [\mu_1 - \mu_2](\text{mod } 1)$	0.40	0.40	0.40	0.40	0.10	0.10	0.10	0.51	0.51	0.51
$\bar{\mu} = [\mu_1 - \Delta/2](\text{mod } 1)$	0.77	0.69	0.63	0.56	0.92	0.85	0.80	0.605	0.545	0.525

points on the unit square. The choice of signs for the plot follows the convention established by Lu and Fano [22]. The neglect of the integers in the ν_i for the purposes of such plots is a reflection of the fact that Eq. (2) is invariant to changes in the values of ν_i by integers. This form of the plot facilitates a fitting of the surface Σ (here a curved line) to the experimental data.

In Fig. 3 we present Lu-Fano plots for Ca, Sr, and Ba. The points correspond to the experimentally measured energies of the $^1P_1^o$ spectra with the following omissions. First, the lowest state in each atom is excluded because MQDT does not apply unless one electron has a large orbit. Next, the highest members of the series ($n > 25$) for Ca and Sr are left off the plots to avoid visual bunching as the *ns* ionization limits are approached. Note that only the lowest member of the perturbing series, 3d4p in Ca and 4d5p in Sr, is bound for these two atoms. For Ba the situation is more complicated. There are several perturbing configurations in the bound portion of the spectrum. The two lowest members of the 5d*n*p channel (5d6p and 5d7p) are completely bound, while the next member (5d8p) is mixed into the 6s*n*p channel in both the bound and continuum regions of the spectrum. This last state is therefore excluded for our present purposes of comparison with Ca and Sr. Finally, the presence of 5d4f perturbers in Ba has no analogue in Ca and Sr, so we only consider Ba states that are not influenced by the 5d4f configuration. Thus, the plot for Ba shows data limited to the energy region below the 6s11p state in Ba.

In any two-channel problem, the unitary matrix $U_{i\alpha}$ has only one independent element. It is convenient to express it in terms of the parameter Θ, with $U_{12} = \sin\Theta$. Figure 3 shows curves that are solutions of Eq. (2) with values for the parameters Θ, μ_1, and μ_2 as given in Table 1 under the heading $^1P_1^o$. Note that the intersections of the upper-left to lower-right diagonal line ($\nu_1 = \nu_2$) with the curves occur at $\nu_1(\text{mod } 1) = \nu_2(\text{mod } 1) = -\mu_1$ and at $\nu_1(\text{mod } 1) = \nu_2(\text{mod } 1) = -\mu_2$. This is a consequence of Eq. (2), which is seen to have such special solutions. The values of Θ, μ_1, and μ_2 were chosen to give good fits to the data for all three atoms and to demonstrate the point made earlier that the curves (surfaces) Σ would have the same shape in all three atoms. Thus Θ is the same for all curves in Fig. 3, as is $\Delta = \mu_1 - \mu_2$. The only thing that changes in the parametrization is $\bar{\mu} = \mu_1 - \Delta/2$. This is further dramatized by displacing each plot along the diagonal so that the curves are superimposed, as shown in Fig. 4. (In this and succeeding plots of superimposed curves, the ν_i values are not transposed by $\bar{\mu}$, as Eq. (5) would suggest, but by $\bar{\mu} + k$, where k is a constant that displaces the curves into a position in the unit square chosen for its suitability in displaying the data.) Thus, one may compactly represent all of the data on the $^1P_1^o$ series in these atoms by the two common parameters, $\Theta = 0.6$ and $\Delta = 0.4$, and a third parameter $\bar{\mu}$ that is different for each atom. This remarkable result indicates that, to a good approximation, the effect of the configuration interaction on the $^1P_1^o$ spectra of these three atoms is identical when seen from the standpoint of MQDT. The channel interaction is expressed in terms of the two parameters Θ and Δ. The differing values of the average quantum defect $\bar{\mu}$ reflect the differences in size and, correspondingly, polarization and penetration of the core by the Rydberg electron as one goes from Ca to Sr to Ba. These changes in $\bar{\mu}$ are not unlike the changes in the quantum defect characterizing one-electron alkali-metal atoms seen along the series Li, Na, K, Rb, and Cs.

A test of our claim of near-invariance in the configuration interaction among the alkaline earths with low-lying d shell excitations is found by examining data for Ra. Using unpublished data provided by Tomkins [23], we get the Lu-Fano plot also shown in Fig. 3. Data are not available on the lower-lying levels needed to test the region where the theoretical curve is rising but we see that the existing data fit on a curve corresponding to the parameters given in Table 1. This curve is produced by displacing the composite Ca-Sr-Ba curve along the $\nu_1 = \nu_2$ diagonal. We hope to take more data on Ra to test the other portions of the curve; however, it is already clear that the Ra $^1P_1^o$ series substantially fits the picture we are presenting.

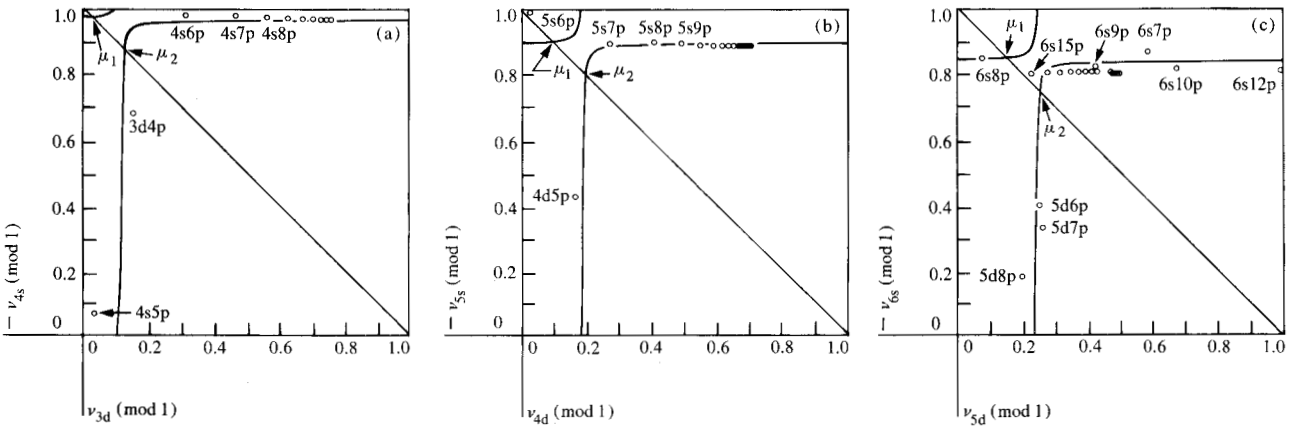

Figure 5 Lu-Fano plots for the bound $^3P_1^o$ spectra of (a) Ca, (b) Sr, and (c) Ba. The curves are MQDT fits using the parameters given in Table 1.

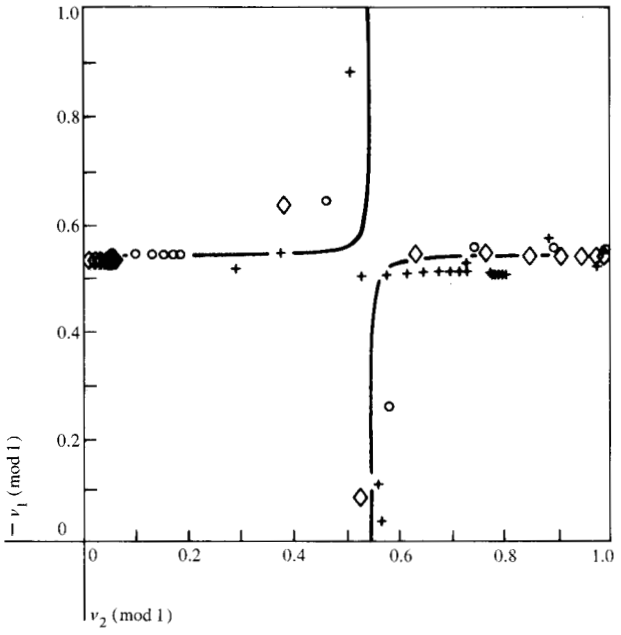

Figure 6 Composite Lu-Fano plot produced by displacing the curves and data of Fig. 5 along the diagonal so as to superimpose the curves. Data points are shown for Ca (○), Sr (◇), and Ba (+).

In fitting the data on the $^1P_1^o$ states, we have not allowed the MQDT parameters to have any energy dependence [15]. If we allow the eigendefect μ_1 to increase with decreasing energy, we can improve the MQDT fits to the experimental data. This additional dependence reflects the fact that low-lying states penetrate and polarize the core more than do high-lying states. For our present purposes, omission of such energy dependence causes the lowest energy states in our plots to deviate from the curves in the Lu-Fano plots in the direction of decreasing ν_1. This will be more obvious in the examples to be considered in the following sections.

$^3P_1^o$ spectra

An examination of the odd-parity $J = 1$ spectra of the alkaline earths shows that the separation into singlet and triplet states is a very good approximation [4]. These series consist primarily of configurations having the core in an S state with no orbital angular momentum and consequently no spin-orbit splitting.

Having already treated the singlet spectra, we now consider the triplet spectra. As in the previous case, the i-channels are described as having the core in the ms state (channel 1) or in the $(m - 1)$d state (channel 2), with the Rydberg electron in a p state for both i-channels. But now the coupling between electrons produces a $^3P_1^o$ state. Following the same procedure as already described, we calculate ν_1 and ν_2 for each state of these spectra in Ca, Sr, and Ba. The results are plotted in Fig. 5. Again, the lowest state in each atom is excluded from the plots. For Ca and Sr, only the lowest member of the perturbing series is bound, while for Ba there are three bound members, 5d6p, 6d7p, and 5d8p. For Ba the 6s11p and 6s13p states are perturbed by 5d4f configurations, while the 6s14p state is perturbed by the 5d8p $^3D_1^o$ state. Since there are no analogous effects in Ca or Sr, these states are omitted from Fig. 5(c).

The solid curves in Fig. 5 are solutions to Eq. (2) obtained by using the values for the various parameters given in Table 1 for the $^3P_1^o$ state. As before, the only differences among the curves are the values chosen for $\bar{\mu}$. Note how the three perturbing states in Ba all lie near the

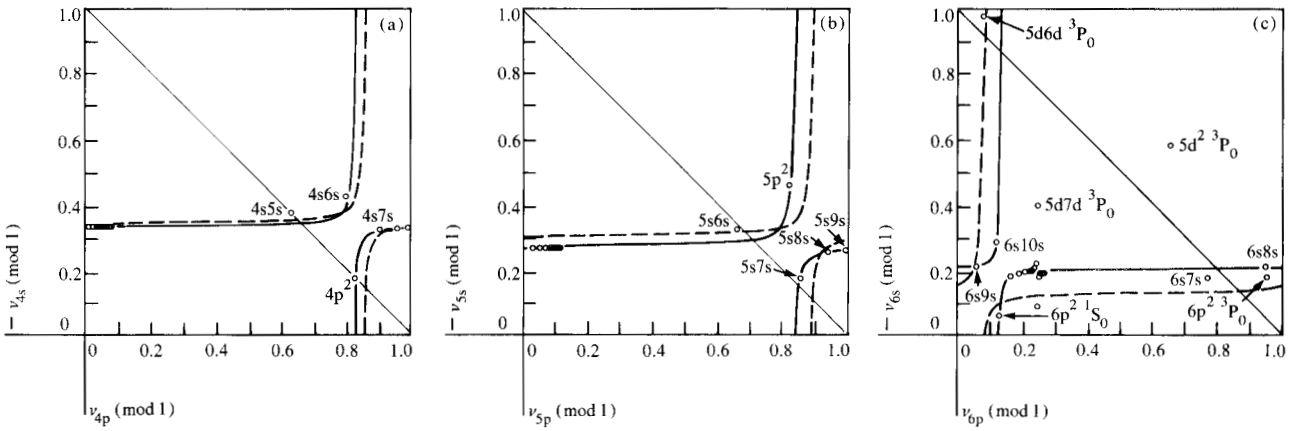

Figure 7 Lu-Fano plots for the bound $^1S_0$ spectra of (a) Ca, (b) Sr, and (c) Ba. The solid curves are MQDT fits using the parameters given in columns 2-4 of Table 2, while the dashed curves use the parameters of columns 5-7 of Table 2.

Table 2 Two-channel MQDT parameters for $^1S_0$ states.

Parameter	*Using I_S and I_P; fitting atoms:*						*Using I_S and I_D; fitting atoms:*					
	Individually			*With common Θ, Δ*			*Individually*			*With common Θ, Δ*		
	Ca	*Sr*	*Ba*	*Ca*	*Sr*	*Ba*	*Ca*	*Sr*	*Ba*	*Ca*	*Sr*	*Ba*
Θ	0.22	0.35	0.10	0.22	0.22	0.22	0.18	0.22	0.28	0.23	0.23	0.23
μ_1	0.35	0.295	0.21	0.36	0.32	0.14	0.335	0.28	0.185	0.345	0.355	0.115
μ_2	0.17	0.145	0.87	0.14	0.10	0.92	0.745	0.82	0.415	0.735	0.745	0.495
$\Delta = [\mu_1 - \mu_2](\text{mod } 1)$	0.18	0.15	0.34	0.22	0.22	0.22	0.59	0.46	0.77	0.61	0.61	0.61
$\tilde{\mu} = [\mu_1 - \Delta/2](\text{mod } 1)$	0.26	0.22	0.04	0.25	0.21	0.03	0.04	0.05	0.80	0.04	0.05	0.80

vertical part of the curve in Fig. 5(c). If we displace each plot along the diagonal to superimpose the curves, we get the composite plot shown in Fig. 6. While the result is not as good a fit to the data as the $^1P_1^o$ case, it still shows how remarkably similar the effects of electron correlation are in all three atoms. Once again, the channel interaction is nearly the same, with only the average quantum defect $\tilde{\mu}$ changing substantially.

An interesting observation is that the configuration interaction is much stronger in the singlet than in the triplet spectrum. In terms of the Lu-Fano plots, this appears as a much larger gap between the two branches of the curves at their distance of closest approach. We interpret this to be a consequence of the tendency of parallel-spin electrons (forming triplet states) to avoid one another, as compared to electrons with antiparallel spins (forming singlet states). If the outer electrons avoid one another, the intermixing of configurations due to Coulomb repulsion between these two electrons is diminished. Hence, a smaller configuration interaction results. Further discussion on this result may be found in Ref. [4]. We shall see that this result is also a feature of the even-parity $J = 2$ spectra.

The separation of the odd-parity Ba $J = 1$ spectrum into singlet and triplet spectra, followed by two-channel MQDT treatments, is an approximation that is made for our present purposes. Note, however, that we have successfully analyzed the complete Ba odd $J = 1$ spectrum with an eight-channel MQDT fit, which includes the effects of the 5d4f states [4]. A discussion of the detailed eight-channel fit is outside the scope of this paper.

● *$^1S_0$ spectra*

For this group of spectra the main series of interest are the *msns* states that have only one even-parity $J = 0$ term, the $^1S_0$. As we shall see, there is more than the usual uncertainty in labeling the perturbers actually seen in the bound $^1S_0$ spectra. The configurations mp^2 or $(m - 1)d^2$, the lowest members of the possible perturbing series, contribute to these perturbers.

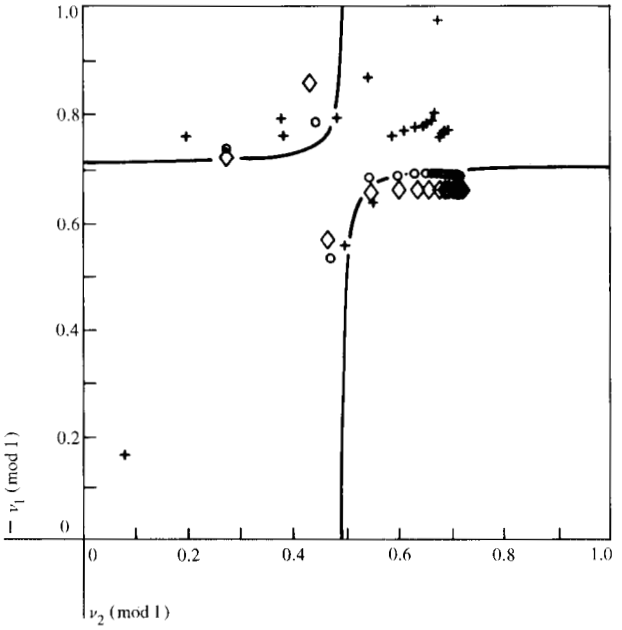

Figure 8 Composite Lu-Fano plot produced by displacing the dashed curves and data of Fig. 7 along the diagonal so as to superimpose the curves. Data points are shown for Ca (○), Sr (◇), and Ba (+).

The bound state region of Ca has been extensively studied by Armstrong *et al.* [2]; that of Sr, by Esherick [3] and Ewart and Purdie [6]; and that of Ba, by Rubbmark *et al.* [7] and Aymar *et al.* [8]. The data for Ca and Sr show a main series with relatively constant quantum defect and a single perturbing level that has been labeled mp^2 in the literature [1]. There is no evidence for another $^1S_0$ perturber in the bound spectra of Ca and Sr. Recent calculations by Nesbet and Jones [24] on Ca predict that $4s^2$, $4p^2$, and $3d^2$ are heavily admixed in the $^1S_0$ spectrum. Their results indicate that the $4s^2$ configuration dominates the ground state but that $4p^2$ and $3d^2$ occur with nearly equal weight in the two other states that have these labels. Their calculation predicts one such state with an energy in excellent agreement with the state traditionally labeled $4p^2$, while the other state (''$3d^2$'') is found to lie well above the 4s ionization limit. This is consistent with the experimental results that show only a single perturber in the bound region of the spectrum.

We present Lu-Fano plots for the $^1S_0$ spectra of Ca and Sr in Figs. 7(a) and (b). The data are taken from Refs. [2] and [3]. In these plots channel 1 has an ms core and an s Rydberg electron, while channel 2 has an mp core and a p Rydberg electron; $I_{^2S_{1/2}}$ is chosen for I_1, while the average of $I_{^2P_{1/2}}$ and $I_{^2P_{3/2}}$ is chosen for I_2, where these labels refer to the ion ground state and the first excited state, respectively. The states so labeled are those that have the highest amount of mp^2 perturber when the data are treated with two-channel MQDT fittings.

The data for Ba are not so straightforward. There are several perturbers of the $6sns$ series in the bound region and their identification is somewhat in question. The data are presented in a Lu-Fano plot in Fig. 7(c), where the average ^2P limit is used for I_2. This plot shows several points well removed from the horizontal line near $-\nu_{6s} = 0.21$, where most of the data lie. These points correspond to the perturbers, and we will shortly present a labeling scheme based on comparisons with Ca and Sr.

We first find two-channel, two-limit MQDT parametrizations for Ca and Sr. Solid curves corresponding to such parametrizations (see columns 2 and 3 in Table 2) are given in Figs. 7(a) and (b). The data on Ba [Fig. 7(c)] show a region near the lower left corner of the Lu-Fano plot where a gap, analogous to that of Ca and Sr, might occur between the two branches of a two-channel fit. This suggests that such a gap is due to the $6p^2$ configuration. With appropriate values for the parameters (column 4 in Table 2), we generate the solid curve shown in Fig. 7(c). The fit is seen to be reasonable if one ignores the three points labeled $5d^2$, 5d6d, and 5d7d $^3P_0$.

We see that all three parameters Θ, Δ, and $\bar{\mu}$ differ in the three atoms when one tries to fit each atom by itself (columns 2–4 in Table 2). If we look for values for Θ and Δ that are common for these atoms we get the results shown by the dashed curves in Fig. 7. The parameters are given in columns 5–7 of Table 2. Displacement of these curves and the data along the $\nu_1 = \nu_2$ diagonal to superimpose the curves produces the composite plot of Fig. 8. While this fit of all three atoms with a curve of the same shape leaves much to be desired, our comparison affords evidence for an identification of $6p^2\ ^1S_0$ for the state in Ba so labeled in Fig. 7(c). This state was labeled 5d6d $^1S_0$ by Aymar *et al.* [8] on the basis of their four-channel MQDT parametrization. However, they ended up without a $6p^2\ ^1S_0$ state. Our label is in basic agreement with Rubbmark *et al.* [7], although they reverse the 6s10s and $6p^2$ labels as compared to us. The state we label 6s8s, in agreement with Rubbmark *et al.*, has been labeled $6p^2$ in the pre-laser tabulations [1].

As an alternative to our choice of the $6p^2\ ^1S_0$ perturber, we consider the possibility that this state is the $5d^2\ ^1S_0$ and the corresponding perturbers in Ca and Sr are $3d^2$ and $4d^2$, respectively. Thus we plot the data using the average of the D-limits for I_2. The results are shown in Fig. 9, where the solid curves correspond to the two-channel parameters of Table 2 (columns 8–10), while the dashed curves

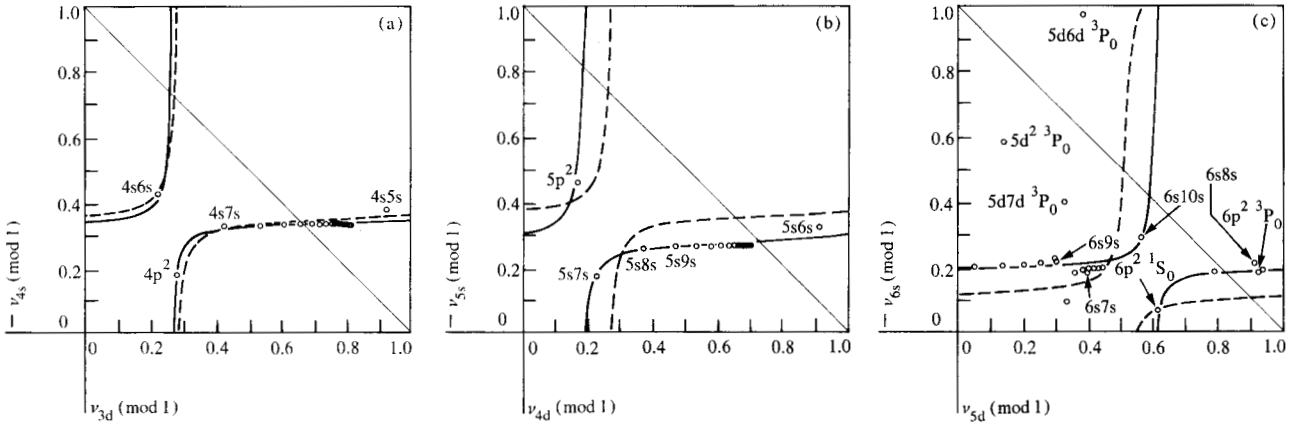

Figure 9 Lu-Fano plots for the bound $^1S_0$ spectra of (a) Ca, (b) Sr, and (c) Ba. The solid curves are MQDT fits using the parameters given in columns 8–10 of Table 2, while the dashed curves use the parameters given in columns 11–13 of Table 2.

have common values of Θ and Δ (see columns 11–13 in Table 2). (Note that the states are still labeled according to the scheme adopted for Fig. 7.) Displacement of the dashed curves and the data along the $\nu_1 = \nu_2$ diagonal produces the composite plot shown in Fig. 10. This composite fit appears to be marginally worse than that of Fig. 8.

The question arises as to which is the better choice of labels, mp^2 or $(m-1)d^2$. The heavy admixture of ms^2, mp^2, and $(m-1)d^2$ into three different $^1S_0$ states in each atom ought to depend strongly on the details of the wave functions of each configuration in the core. Since these configurations all correspond to tightly bound as opposed to Rydberg electrons, MQDT should be inadequate in describing the interactions and admixtures. In the absence of data that could give information about the interactions between these configurations, such as autoionizing spectra, we have insufficient information to make a choice between mp^2 and $(m-1)d^2$. The reader may draw his own conclusions from a comparison of Figs. 8 and 10. In general, the $^1S_0$ spectra show much less striking evidence for systematic near-invariance in the MQDT parameter set than do the $^1P_1^o$ and $^3P_1^o$ spectra. We believe this reflects a particular difficulty that MQDT encounters in describing electron-electron interactions between electrons *in the same orbit*.

As for the other perturbers, the labels given in Fig. 7(c) agree with those of Moore [1] and Aymar *et al.* [8]. Thus the $5d^2$, 5d6d, and 5d7d configurations are present as $^3P_0$ states in the bound region. Only the 5d7d $^3P_0^o$ state has an observable effect on the 6s*n*s $^1S_0$ series. Since no comparable effects are seen in Ca and Sr, we do not treat this state or the appropriate channels in our MQDT fits.

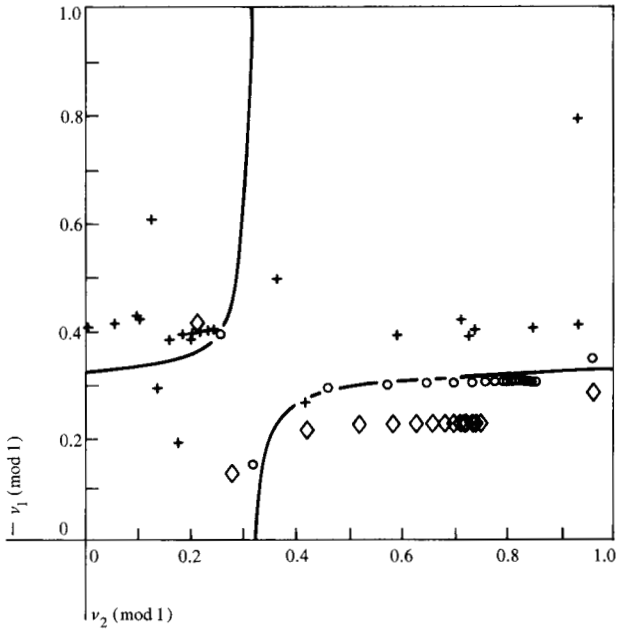

Figure 10 Composite Lu-Fano plot produced by displacing the dashed curves and data of Fig. 9 along the diagonal so as to superimpose the curves. Data points are shown for Ca (○), Sr (◇), and Ba (+).

• $^3D_2$ *spectra*

We next turn to the $^3D_2$ spectra, with the main series being the *ms*n*d* states. Possible perturbing series are *mpn*p, $(m-1)$d*n*s, and $(m-1)$d*n*d. The bound state data for Ca are given up to 4s16d in Moore's tables [1]. We did not observe many $^3D_2$ states in our studies [2] because singlet-to-triplet transitions were very weak due to the small spin-orbit interaction in Ca. However, many more

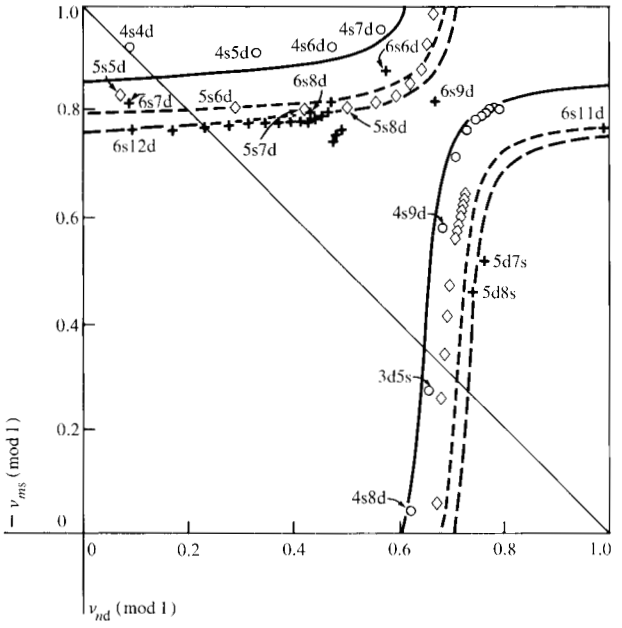

Figure 11 Lu-Fano plots for the bound $^3D_2$ spectra Ca (——, ○), Sr (- - -, ◇), and Ba (— —, +). The curves are MQDT fits using the parameters given in Table 1.

$^3D_2$ states in Sr were seen by Esherick [3] in our laboratory. Rubbmark *et al.* [7] and Aymar *et al.* [8] studied the $^3D_2$ states in Ba, and Aymar and Robaux [17] have published an MQDT analysis of the data of Aymar *et al.* [8].

The data for Ca and Sr show evidence for the presence of a single perturbing level whose influence is distributed over many members of the *msn*d series. In Ca, the singlet-triplet interaction is sufficiently weak that singlets and triplets may be treated in a completely decoupled manner. The MQDT analysis of Ca in Ref. [2] showed that while the Σ surfaces for the $^1D_2$ and $^3D_2$ series cross in several places, the real states near these crossing points show no evidence of these crossings. In contrast, the analysis of Sr in Ref. [3] shows clear evidence of an avoided crossing between the $^1D_2$ and $^3D_2$ surfaces, with several states having nearly equal amounts of $^1D_2$ and $^3D_2$ character. Despite this, over most of the spectrum the triplets and singlets may be distinguished in Sr.

We present Lu-Fano plots for the bound $^3D_2$ spectra of Ca and Sr in Fig. 11. In these plots channel 1 has an *ms* core and a d Rydberg electron, while channel 2 has an $(m-1)$d core and an s Rydberg electron. An average of $I_{^2D_{3/2}}$ and $I_{^2D_{5/2}}$ is chosen for I_2. The state so labeled for Ca is that with the highest amount of 3d5s perturber when the data are analyzed with MQDT. The analogous configuration, 4d6s in Sr, is so diluted throughout the 6s*n*d series that no state has more than eight percent 4d6s $^3D_2$ character. Thus, no individual state can be appropriately given this label [3]. The choice of the $(m-1)$d*n*s channel as the perturbing channel is based on the following reasoning: 1) there is only a single perturber and 2) it cannot be the lowest member of the *mpnp* or $(m-1)$d*n*d channels, since these are the *m*p^2 and $(m-1)$d^2 states, respectively, and neither can have a $^3D_2$ term by the Pauli exclusion principle. Note that in contrast to the $^1S_0$ spectra, and in analogy to the $^1P_1^o$ and $^3P_1^o$ spectra, neither the main channel *msn*d nor the perturbing channel $(m-1)$d*n*s has states with both electrons in the same orbit.

The data for Ba are, once again, more complicated. The analysis of Aymar and Robaux (17) identifies the following states as having significant perturbing effect on the 6s*n*d $^3D_2$ spectrum; 5d7s $^3D_2$, 5d8s $^3D_2$, 6p^2 $^1D_2$, 5d8s $^1D_2$, and 5d7d $^1D_2$. The analysis of Aymar and Robaux also gives labels to many other perturbers, but these others do not appear to significantly influence the 6s*n*d $^3D_2$ spectrum. The state labeled 6p^2 $^1D_2$ has only a weak influence so we omit it. Similarly, the influence of the state labeled 5d8s $^1D_2$ on the triplets is confined to the 6s10d $^3D_2$ state. To facilitate our comparison with Ca and Sr, we omit both of these states. The 5d7d $^1D_2$ influences the triplet spectrum through its perturbation of the 6s*n*d $^1D_2$ series, forcing it to cross the $^3D_2$ series. This leads to an easily observed avoided crossing between singlets and triplets. For present purposes, the 5d7d $^1D_2$ perturber is omitted. The balance of the $^3D_2$ spectrum of Ba is presented in a Lu-Fano plot in Fig. 11, using the average of the ^2D limits for I_2. The two perturbers 5d7s and 5d8s fall away from the horizontal line near $-\nu_s = 0.78$, where most of the other data points lie. In all three plots of Fig. 11, the lowest members of the main series are, as usual, omitted.

Curves corresponding to two-channel, two-limit MQDT parametrizations for all three atoms (using the values given for the $^3D_2$ states in Table 1) are also presented in Fig. 11. While the curves for Ca and Sr nicely reproduce the pattern shown by the data, Ba requires additional explanation. Due to the influence of the state labeled 6p^2 $^1D_2$ by Aymar and Robaux, the 6s9d $^3D_2$ state is pushed to higher energy, causing it to lie off the curve. The higher *n* states show the effects of the 5d7d $^1D_2$ state mentioned earlier. Other than that, the two-channel curve reproduces the Ba data nicely, allowing for the usual deviation of the lowest-lying states (6s6d and 6s7d in this case) from the curve. In particular, both the 5d7s and 5d8s perturbers lie very close to the vertical portion of the curve.

The curves given in Fig. 11 have all used the same value for Θ and Δ, as in the previous cases. Displacement of the curves and the data along the $\nu_1 = \nu_2$ diagonal to

superimpose the curves produces the composite plot of Fig. 12. Once again, the behavior of all three atoms is remarkably similar.

• $^1D_2$ *spectra*

For this group of spectra the main series are again the *msnd* states. However, this situation is much more complicated than the $^3D_2$ spectra because the *mpnp* and $(m-1)$d*nd* channels *do* influence the $^1D_2$ spectra and because the perturbing channels include states with two electrons in identical orbits. The bound state regions of Ca and Sr were extensively studied in our laboratory [2, 3]. Rubbmark *et al.* [7] and Aymar *et al.* [8] studied Ba, with Aymar and Robaux [17] carrying out an MQDT analysis.

To treat the Ca and Sr data, we first neglect the spin-orbit splitting of the ^{2}D and ^{2}P core states, leaving a three-limit problem. This is consistent with the separation of the data into singlets and triplets mentioned earlier. In a three-limit case the MQDT approach yields three values of ν_i for each state. The corresponding Lu-Fano plots are three-dimensional [2]. We present a stereo view of a three-dimensional Lu-Fano plot of the $^1D_2$ data of Ca [2] and Sr [3] in Fig. 13. (For help in viewing stereo figures, see the figure caption.) For comparison to theory, the Sr data has been displaced -0.05 along the ν_i-space body diagonal. The points that are next-to-nearest to the right-hand face of the cube correspond to the states traditionally labeled mp^2 [1]. The other perturbers are so diluted throughout the *msnd* series that no individual states merit the $(m-1)$d$(m+1)$s or md^2 labels. In the case of Sr the $4d^2$ perturber lies entirely in the continuum above the I_S limit and appears as an autoionizing state [3].

A surface Σ corresponding to four-channel, three-limit MQDT parametrizations, using the values for Ca in Table 3, is also presented in Fig. 13. In this MQDT analysis channel 1 has an *ms* core and a d Rydberg electron, channel 2 has an $(m-1)$d core and an s Rydberg electron, channel 3 has an $(m-1)$d core and a d Rydberg electron, and channel 4 has an *mp* core and a p Rydberg electron. Instead of showing the surface translated into the unit cube where it would have many sheets (branches) and look very confusing, we have displayed one continuous sheet covering a range for $-\nu_s$ of 0.72 to 3.72, while ν_d and ν_p vary from 0 to 1.0. Here, instead of displacing the surface Σ along the ν_i-space body diagonal a distance 0.05 in going from Ca to Sr, we have displaced the Sr data -0.05 to produce a composite plot.

This figure dramatically illustrates the fact that the surfaces Σ_{Ca} and Σ_{Sr}, in which the respective $^1D_2$ states lie, *differ only by translation along the body diagonal.* The shapes of the two surfaces are identical. This exhibits the invariance of the channel interactions from atom to atom within a spectral class for a many-channel, many-limit case.

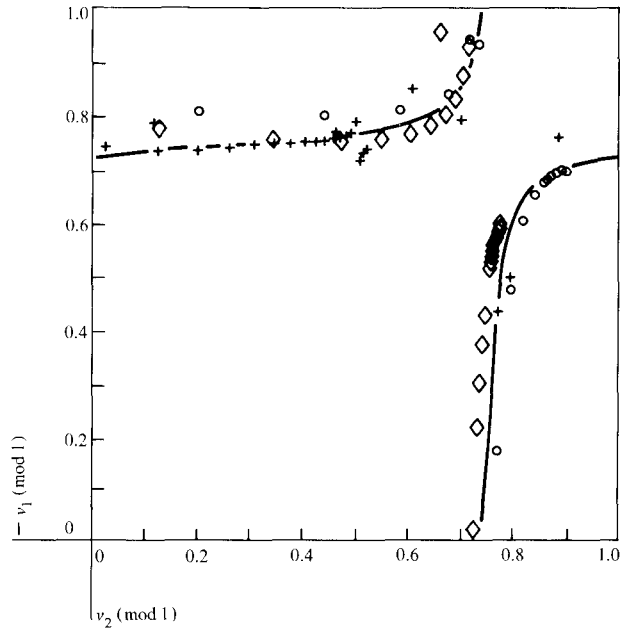

Figure 12 Composite Lu-Fano plot produced by displacing the curves and data of Fig. 11 along the diagonal so as to superimpose the curves. Data points are shown for Ca (○), Sr (◇), and Ba (+).

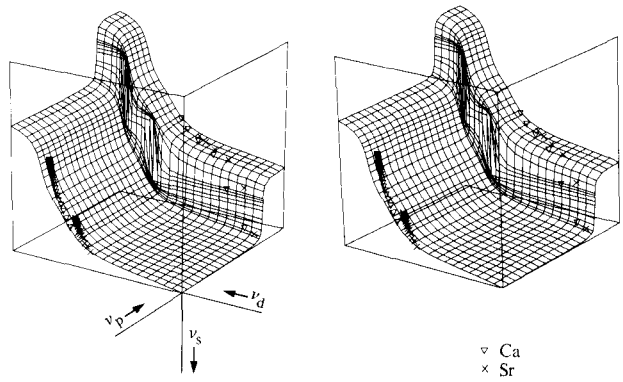

Figure 13 Stereo Lu-Fano plot for the bound $^1D_2$ spectra of Ca and Sr. The surface is a four-channel MQDT fit to Ca using the parameters given in Table 3. The Sr data points have been moved -0.05 along the body diagonal to lie in or near the surface. The three axes are dimensionless with $-\nu_s$ values running from 0.72 to 3.72, and ν_d and ν_p running from 0 to 1.0. If no stereo viewer is available, place the figure about one foot from your eyes, place an obstruction between your eyes so that each eye can see only one image, and then fuse the two images.

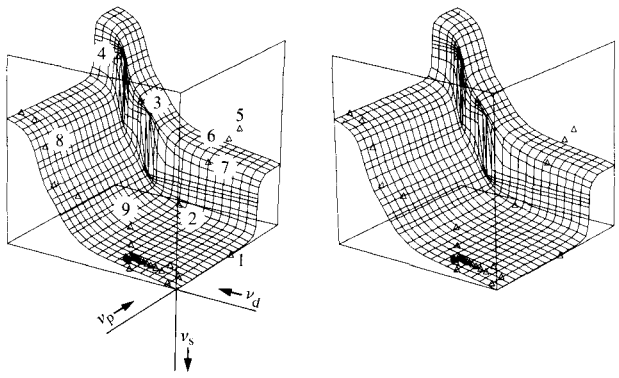

Figure 14 Stereo Lu-Fano plot for the bound $^1D_2$ spectrum of Ba. The surface corresponds to the Ca parameters of Table 3. The data points have been moved −0.12 along the body diagonal to lie near the surface.

Table 3 Four-channel MQDT parameters for $^1D_2$ states using I_S, I_D, and I_P.

Parameter				
i, α	1	2	3	4
$\|i\rangle$	$[ms]d$	$[(m-1)d]s$	$[(m-1)d]d$	$[mp]p$
I_i	I_S	I_D	I_D	I_P
$\mu'_\alpha = [\mu_\alpha - \tilde{\mu}]^\dagger (\text{mod } 1)$	0.43	0.95	0.79	0.83
$U_{i\alpha}$; $i = 1$	0.837	−0.444	−0.301	−0.109
$i = 2$	0.415	0.896	−0.149	−0.054
$i = 3$	0.333	0	0.942	−0.044
$i = 4$	0.130	0	0	−0.992

$^\dagger \tilde{\mu}_{Ca} = 0.39$, $\tilde{\mu}_{Sr} = 0.34$, $\tilde{\mu}_{Ba} = 0.27$.

Turning to Ba, we find once again a more complicated situation. First, Ba has several members of the perturbing series 5d*n*s and 5d*n*d occurring in the bound region of the spectrum. Next, the spin-orbit splitting of the D core is sizeable (800 cm^{-1}), making the separation into singlet and triplet states questionable. Perturbers with singlet and triplet labels are both found to perturb the 6s*n*d $^1D_2$ spectrum. Next, in the spectral region from the 6s6d to 6s11d $^1D_2$ states, there are ten perturbing levels according to the labeling scheme of Aymar *et al.* [8]. This confuses the spectrum and makes any labeling scheme quite speculative. Finally, the lowest members of some of the perturbing channels have configurations with identical electrons, *i.e.*, mp^2. Such states do not satisfy the MQDT criterion of having a highly excited Rydberg electron. This is a problem with Ca and Sr as well.

With these problems in mind we took the Ba data [8] and translated the corresponding points in three-dimensional ν_i-space along the body diagonal to see how nearly the data would lie in the surface Σ that contains the data points for Ca and Sr. The result is shown in Fig. 14, where the Ba data have been displaced −0.12 along the diagonal. The ν_s(mod 1) values have had the integers 1 or 2 added to them to move them close to that part (sheet) of Σ we have plotted. While the fit is not as good as for Ca or Sr, the majority of the points lie close to the same surface. In particular, the points along the left-most contours follow the shape of the surface remarkably well. The points indicated by the numbers 1 to 9 have been labeled by Aymar and Robaux [17] as $^1D_2$ states with the following configuration: 1-5d^2, 2-6s6d, 3-5d7s, 4-6s7d, 5-6s8d, 6-5d6d, 7-6p^2, 8-5d8s, and 9-5d7d (these are given in order of increasing energy). Of these, 4, 5, 6, and 7 appear to lie farthest away from the surface.

We cannot, on the basis of this three-limit, four-channel fit, propose an acceptable set of assignments for all the $^1D_2$ states. A more complicated fit, including the effects of the spin-orbit interaction and singlet-triplet mixing, is required. However, the comparison with Ca and Sr in the manner we have carried out in this paper casts some doubt on the assignments of Aymar and Robaux [17]. In particular, the 6p^2 state ought to lie near the sharply rising contour at $\approx\nu'_p = 0.78$ (the prime indicates the shift of the data by −0.12 in ν_i-space) rather than near $\nu'_p = 0.99$, as does point 7 in Fig. 14. Similarly, the 5d7s and 5d8s states ought to lie near the gradually rising contour at $\approx\nu'_d = 0.66$, whereas points 3 and 8 have $\nu'_d = 0.73$ and 0.82, respectively. Finally, the 5d^2, 5d6d, and 5d7d states ought to have $\nu'_d = 0.82$, whereas points 1, 6, and 9 have $\nu'_d = 0.01$, 0.28, and 0.36, respectively.

This example of the $^1D_2$ states in Ca, Sr, and Ba further highlights the extent to which spectral regularities and invariances are revealed by the point of view and apparatus of MQDT.

Conclusion

We have studied spectral regularities along the series Ca, Sr, Ba (and in one case, Ra). The series studied were $^1P^o_1$, $^3P^o_1$, $^1S_0$, $^3D_2$, and $^1D_2$. For each spectral type, except the $^1S_0$, most states in the observed series can be described quantitatively by a set of MQDT parameters of which all but one are the same for Ca, Sr, and Ba. Even in the series of Ba that have perturbing channels not found in the other atoms, the description appropriate to Ca and Sr is

still found to provide an excellent "starting" description of the spectra for Ba. These points are exemplified in Figs. 4, 12, 13, and 14.

Multichannel quantum defect theory affords a framework with which to describe the channel interactions of two-electron spectra independently of particular values for series limits. This is the significance of the surface Σ, described by Eq. (2). The near-invariance of the surface Σ along the series Ca, Sr, Ba (and Ra?), appropriate to a given spectral type, implies that there are basis sets of two-electron wave functions; *i.e.*, these are basis channels that diagonalize the noncentral Coulomb scattering of the two-electron system, independent of whether one is dealing with Ca, Sr, or Ba. Similarly, there is a set of common eigenphase shifts (eigenquantum defects) μ_α' that belong to a given spectral type. It remains for future work to exhibit these invariances in the more usual non-MQDT treatment of configuration interactions and/or in a group theoretical description of the dynamical symmetries of "two-electron" atoms.

References

1. C. E. Moore, *Atomic Energy Levels*, National Bureau of Standards Circular, No. 467 (U.S. Government Printing Office, Washington, DC), Vol. 1 (1949), Vol. 2 (1952), Vol. 3 (1958).
2. J. A. Armstrong, P. Esherick, and J. J. Wynne, *Phys. Rev. A* **15,** 180 (1977).
3. P. Esherick, *Phys. Rev. A* **15,** 1920 (1977).
4. J. A. Armstrong, J. J. Wynne, and P. Esherick, *J. Opt. Soc. Amer.* **69,** 211 (1979).
5. D. J. Bradley, P. Ewart, J. V. Nicholas, and J. R. D. Shaw, *J. Phys. B* **6,** 1594 (1973).
6. P. Ewart and A. F. Purdie, *J. Phys. B* **9,** L437 (1976).
7. J. R. Rubbmark, S. A. Borgström, and K. Bockasten, *J. Phys. B* **10,** 421 (1977).
8. M. Aymar, P. Camus, M. Dieulin, and C. Morillon, *Phys. Rev. A* **18,** 2173 (1978).
9. W. R. S. Garton and K. Codling, *J. Phys. B* **1,** 106 (1968).
10. W. R. S. Garton and F. S. Tomkins, *Astrophys. J.* **158,** 1219 (1969).
11. C. M. Brown, S. G. Tilford, and M. L. Ginter, *J. Opt. Soc. Amer.* **63,** 1454 (1973).
12. M. J. Seaton, *Proc. Phys. Soc. (Lond.)* **88,** 801 (1966).
13. U. Fano, *Phys. Rev. A* **2,** 353 (1970).
14. K. T. Lu, *Phys. Rev. A* **4,** 579 (1971).
15. C. M. Lee and K. T. Lu, *Phys. Rev. A* **8,** 1241 (1973).
16. U. Fano, *J. Opt. Soc. Amer.* **65,** 979 (1975).
17. M. Aymar and O. Robaux, *J. Phys. B*, accepted for publication.
18. K. T. Lu, *J. Opt. Soc. Amer.* **64,** 706 (1974).
19. K. H. Kingdon, *Phys. Rev.* **21,** 408 (1923).
20. J. P. Hermann and J. J. Wynne, *J. Opt. Soc. Amer.* **68,** 1412 (1978).
21. E. F. Worden, J. A. Paisner, and J. G. Conway, *Opt. Lett.* **3,** 156 (1978).
22. K. T. Lu and U. Fano, *Phys. Rev. A* **2,** 81 (1970).
23. F. S. Tomkins, Chemistry Division, Argonne National Laboratory, Argonne, IL 60439, private communication.
24. R. K. Nesbet and J. W. Jones, *Phys. Rev. A* **16,** 1161 (1977).

Received January 18, 1979; revised March 17, 1979

The authors are located at the IBM Thomas J. Watson Research Center, Yorktown Heights, New York 10598.